# Università degli studi di Udine

## Engineering of metal-MoS2 contacts to overcome Fermi level pinning

(Article begins on next page)

18 December 2025

# Engineering of metal-MoS$_2$ contacts to overcome Fermi level pinning

P. Khakbaz[1], F. Driussi[1], P. Giannozzi[1, 2], A. Gambi[1], D. Lizzit[1], D. Esseni[1]

[1]*Università degli Studi di Udine, via delle Scienze 206, 33100 Udine, Italy*

[2]*CNR-IOM, Istituto dell'Officina dei Materiali, SISSA, I-34136 Trieste, Italy*

*E-mail address of corresponding author: Khakbaz.Pedram@spes.uniud.it*

## Abstract

Fermi level pinning (FLP) in metal-MoS$_2$ contacts induces large Schottky barrier heights which in turn results in large contact resistances. In this work, we made use of Density Functional Theory (DFT) to study the origin of FLP in MoS$_2$ contacts with a variety of metals. We also reported how the Fermi level de-pinning could be attained by controlling the distance between the metal and MoS$_2$. In this respect, the metal-MoS$_2$ contacts can be engineered by means of the insertion of proper buffer layers and the use of back-gated structures. This results in a practically zeroed Schottky barrier heights for some specific metal-MoS$_2$ stacks, which it is crucial to attain Ohmic contacts with low series resistances.

## 1. Introduction and summary

In recent years, the research of new low dimensional materials for electronic applications demonstrated the interesting electrical properties of two-dimensional (2D) transition metal dichalcogenides. Among these 2D materials, MoS$_2$ is the most technologically mature semiconductor [1]. In particular, MoS$_2$ exhibits extreme flexibility and large piezo-resistance [2], which makes it a viable solution for new applications in the field of tactile sensing in soft robotics [3], of electronic skin [4] and fast thermal sensors [5], besides new structures and devices for nano-electronic circuits [6]. All these interesting applications require to attain a high-quality metal-MoS$_2$ contact. However, the reported values for the metal-MoS$_2$ contact resistance are in the k$\Omega \cdot \mu$m range [6], in sharp contrast with the projections of the IRDS roadmap [7], that targets tens of $\Omega \cdot \mu$m for the contact resistance in nanoscale FETs.

The need to optimize the metal-MoS$_2$ heterostructure with the aim of reducing the contact resistance steered the research efforts towards the characterization and detailed analysis of MoS$_2$ contacts with several metal materials [8, 9]. In this respect, the lack of dangling bonds at the MoS$_2$ surface have raised expectations for a weak Fermi level pinning (FLP) at the metal-MoS$_2$ interface. According to the Schottky–Mott rule [10], this would allow for a good control of the Schottky Barrier Height (SBH) between the metal and MoS$_2$ through the selection of the metals with an appropriate work function (WF). However, the experiments indicate that the SBH versus WF curves largely disagree with the Schottky–Mott rule predictions and the slope of these curves is as small as 0.11[11] or 0.09 [12], thus pointing to a large FLP [11]. The FLP observed in the experiments may be mainly caused by defects in the MoS$_2$ structure [11, 13], but even for an ideal MoS$_2$ layer, a large density of metal-induced Interface Gap States (IGS) has been predicted by several reports based on Density Functional Theory (DFT) calculations [14, 15, 16]. Such IGS contribute to the measured FLP in the actual test structures and, moreover, set the best-case scenario for metal-MoS$_2$ systems.

In this work, we extend the work presented in [17] by reporting new DFT results about FLP and SBH in defect-free metal-MoS$_2$ contacts with different metals. In particular, we discuss in depth the conditions favoring the Fermi level de-pinning, which is crucial to open the possibility to engineer the SBH and thus attain an Ohmic behavior of the metal-MoS$_2$ contacts. In this respect, we here studied also possible buffer layers that could be inserted between MoS$_2$ and the metal contact, eventually allowing for the suppression of IGS and, thus, for the Fermi level de-pinning. We revised the electrical behavior of such contacts exploiting buffer layers, highlighting those that could eventually ensure a zero SBH and the direct electrical contact to the Conduction Band (CB) or the Valence Band (VB) of the MoS$_2$.
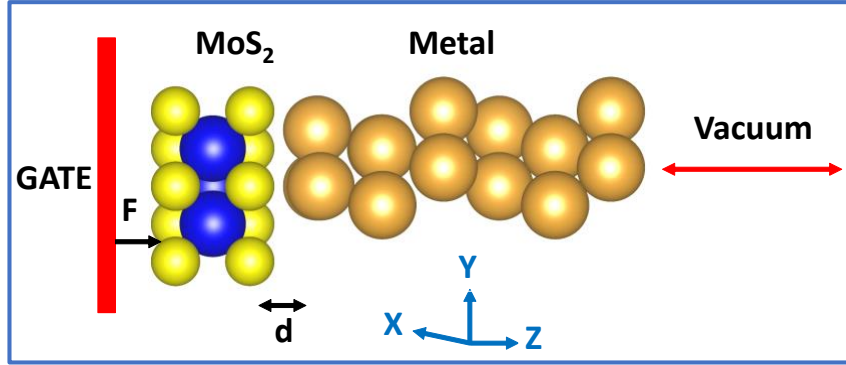
*Fig. 1: Simulation method used through this work: the metal-MoS$_2$ stack is fully relaxed. Here d is the metal-MoS$_2$ distance. A back gate is included to bias the system and to induce an external electric field F across the contact structure.*

## 2. DFT simulation methodology

In this work, we made use of the DFT methodology, as implemented in the Quantum ESPRESSO suite, to study the MoS$_2$ in contact with aluminum (Al), gold (Au) and palladium (Pd) [17, 18]. For these three contact options, we produced supercells sandwiching a MoS$_2$ monolayer with a metal crystal formed by six layers of metal atoms as sketched in Fig. 1.

The simulated supercells include also a 1.5 nm thick vacuum region along $z$ at the metal side of the heterostructure (Fig. 1). We used the dipole correction procedure to minimize the spurious coupling between the periodic replicas of the supercell [18]. We employed the PBE (Perdew−Burke−Ernzerhof) exchange-correlation functionals and the electron−ion interactions were described through the projector augmented-wave (PAW) pseudopotentials. Van der Waals forces have been included adopting the DFT-D3 corrections. In order to be able to apply an electric field to the heterostructure along the $z$ direction, we also added a back-gate at the MoS$_2$ side of the system (see Fig. 1) [19, 20, 21].

For the analyzed systems, in order to minimize the strain along the $x$-$y$ plane parallel to the interface (see Fig. 1), we matched the 111-surface of a six-layer metal crystal to a $\sqrt{3} \times \sqrt{3}$ supercell for the monolayer MoS$_2$ [15]. Then, we also used relaxation to reduce residual forces on atoms [22] and, in particular, we relaxed the position of all the atoms in the system [17]. We believe that this approach is more dependable than some procedures previously reported in the literature, where the position of the four top metal layers were instead fixed and the relaxation was involved only the metal layers close to the MoS$_2$ semiconductor [14, 15]. Indeed, our procedure prevents the formation of charge dipoles inside the metal crystal. In [17] we demonstrated that a non-completely relaxed structure may lead to overlooked artifacts in the dipole analysis and in the calculations of the SBH in metal-MoS$_2$ contacts.

The relaxation of the whole stack allowed us to obtain the minimum energy distances (MD) between MoS$_2$ and the different metals. In particular, we obtained MD = 0.3 nm for the Au contact, MD = 0.27 nm for the Al contact and MD = 0.25 nm for the Pd contact, which are in fairly good agreement with the values reported in literature [15]. Furthermore, we verified that the calculated band structures of isolated MoS$_2$, Au, Al and Pd are also in good agreement with literature data [15].

## 3. Fermi level pinning and interface states

With the aim of studying the presence of the FLP, its physical origin and the possible impact on the SBH at the metal-MoS$_2$ interface, we have calculated the density of states projected on the MoS$_2$ layer (PDoS) for the supercells of the different contacts to MoS$_2$ described above and then we have compared the PDoS with the DoS of the free standing MoS$_2$ (Fig. 2(d)). In particular, for each metal option, we evaluated the PDoS for different distances, $d$, between the MoS$_2$ monolayer and the metal (see Fig. 1) and we inspected the position of the Fermi level with respect to the conduction band (CB) and valence band (VB) edges of MoS$_2$.

Figure 2 reports the results obtained for the MoS$_2$-Au contact. In this graph and in the following ones, the PDoS is plotted by taking the Fermi level ($E_F$) of the heterostructure as the energy reference. Moreover, we defined and extracted the SBH for electrons/holes ($\Phi_e$ / $\Phi_h$) as the difference between the CB/VB edge and $E_F$ [14]. It is worth noting that for $d = 0.8$ nm [Fig. 2(a)], the PDoS of the MoS$_2$ layer is consistent with the isolated material (the energy gap is $E_{gap} \approx 1.8$ eV) [23], with no evidence of IGS inside the bandgap of the MoS$_2$. Furthermore, the calculated SBH agrees well with the Schottky–Mott rule when assuming a work function of about WF = 5.5 eV for the Au contact and an affinity of about 4.2 eV for MoS$_2$ [22, 24]. Indeed, the large WF of Au results in a smaller the SBH for holes (that however it is still large) compared to the SBH for electrons.

Figures 2(b) and (c) show the extracted MoS$_2$ PDoS for shorter $d$ values; in these cases, instead, it is possible to observe the appearance of the IGS inside the bandgap of the MoS$_2$, having a not at all negligible density. This results in the pinning of the Fermi level inside the MoS$_2$ bandgap, as testified by the change in the position of the VB and CB edges, which affects the SBH between the Au and MoS$_2$. At the minimum energy distance, in particular, the $E_F$ position is strongly pinned around mid-gap, thus resulting in a large SBH for both holes and electrons. This latter result well agrees with direct measurements of the monolayer MoS$_2$ on Au (111) band structure through ARPES technique, which report a position of the top of the valence band at about 1.3 eV from $E_F$ [25].

Similar results are observed for the Pd contact, another high WF metal material, possibly suitable to produce a $p$-type contact to the MoS$_2$. Figure 3 reports in semi-logarithmic scales the PDoS for the MoS$_2$-Pd system for different $d$ values. Again, by shortening the distance between the metal and the semiconductor, there is a large increase in the density of the IGS, that completely distorts the band structure of MoS$_2$ at the MD (black line). For this system, it is also difficult to calculate the SBH at small $d$, because the PDoS of the MOS$_2$ is largely affected by the presence of Pd. Because of the similarity of the results obtained for contacts based on Pd and Au, we will not explicitly show the results for the Pd-MoS$_2$ system in the remaining part of the manuscript.
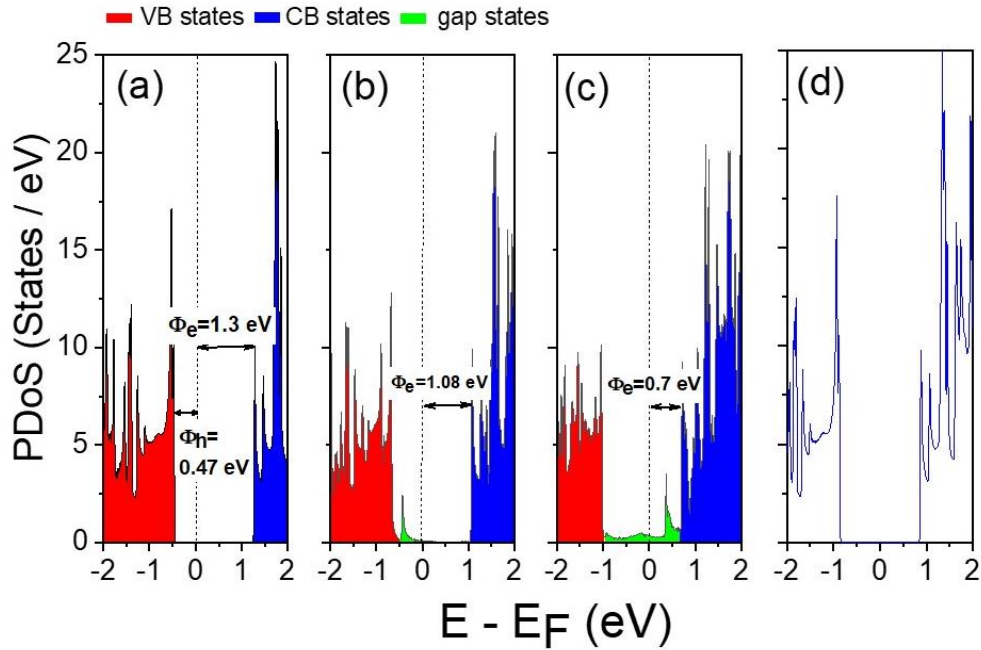


*Fig. 2: PDoS of MoS$_2$ in the MoS$_2$-Au stack for (a) d=0.8 nm, (b) d=0.4 nm and (c) d=0.3 nm (MD). At short distances and, in particular, at the MD, we see the onset of IGS (marked in green) that pin the Fermi level $E_F$ inside the bandgap. (d) DoS of isolated MoS$_2$.*
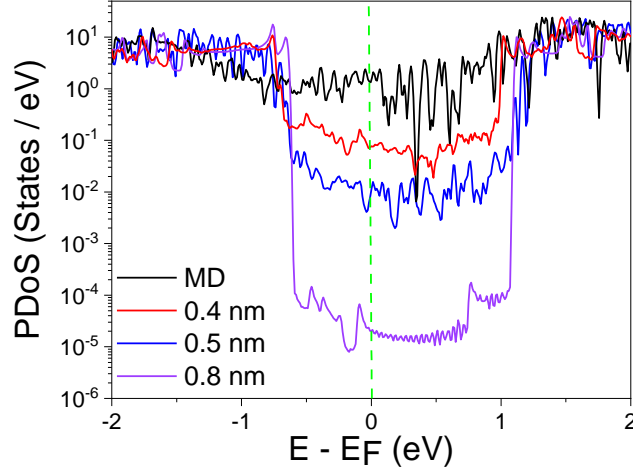
*Fig. 3: PDoS of MoS₂ in MoS₂-Pd stack for different d values in logarithmic scales. At the MD, there is a very large density of IGS inside the bandgap (black line), which completely distorts the band structure of MoS₂. By increasing d, instead, the IGS density is suppressed.*
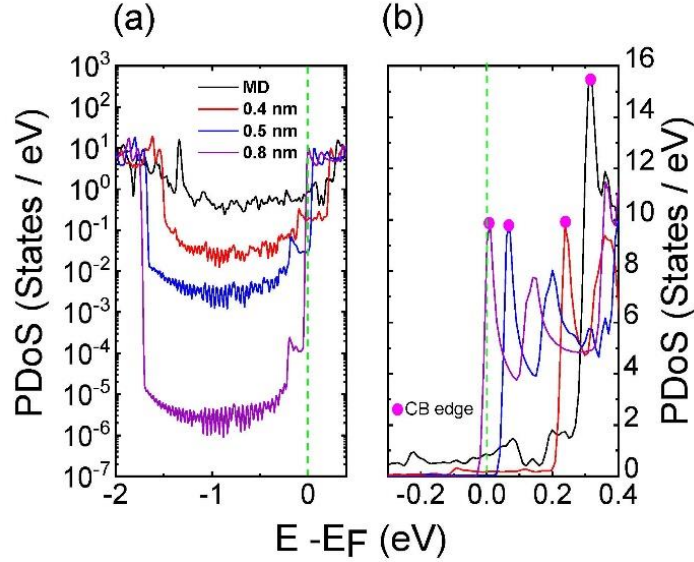


*Fig. 4: PDoS of MoS₂ in MoS₂-Al stack for different d values in logarithmic (**a**) and linear scales (**b**), zoomed around $E_F$. For MD, $E_F$ is pinned well inside the MoS₂ bandgap due to IGS (black line). By increasing d, the IGS density is suppressed, so that $E_F$ gets de-pinned and reaches the MoS₂ CB for d=0.8 nm.*

The case of the MoS₂-Al stack, which is shown in Fig. 4, is instead much more interesting. In this case the Al electrode features a small WF value of about 4 eV [15]. This should ease the electrical contact to the CB of MoS₂. However, in Fig. 4(a), we observe a large PDoS increase inside the MoS₂ bandgap at small $d$ values, which strongly pins $E_F$ well far from the CB edge and results in a large SBH for electrons, which is best illustrated by Fig. 4(b). For $d = 0.8$ nm, instead, the presence of IGS is largely suppressed [purple line in Fig. 4(a)], so the Fermi level gets de-pinned and the observed SBH for electrons is approximately zero, as expected accordingly to the Schottky–Mott rule and the WF = 4 eV of the Al slab.

## 4. Back-gating of the MoS₂ contacts

As already widely observed experimentally for the graphene contacts [19], the use of a back-gate may favor the reduction of the series resistance also for the metal-MoS₂ contacts [26, 27]. Therefore, as sketched in Fig. 1, we included in the simulated system a back-gate able to induce an external electric field ($F$) along the direction $z$ normal to the contact plane, thus allowing the biasing of the MoS₂.
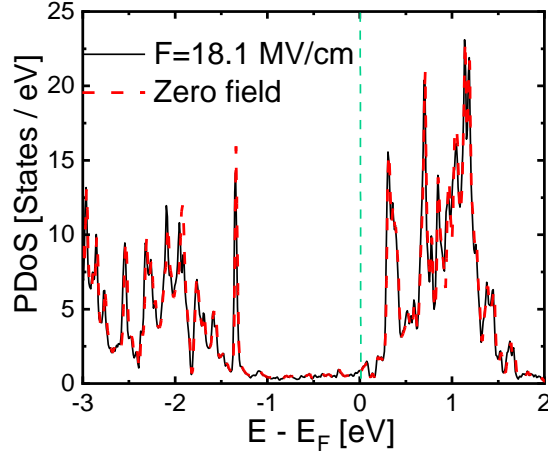
*Fig. 5: PDoS of MoS₂ obtained from the MoS₂-Al system featuring the back gate and by considering the MD. The applied external electric field is F = 0 and 18.1 MV/cm. $E_F$ is strongly pinned and the electric field induced by the back gate cannot influence the $E_F$ position.*

Figure 5 reports the DoS projected on MoS₂ for the Al contact at the minimum energy distance with or without the externally-applied electric field. As it can be seen, the strong FLP for MD precludes any SBH modulation. Figure 6 shows that, instead, for the enlarged distance $d = 0.8$ nm, because of the $E_F$ depinning favored by the IGS suppression, the field can effectively shift $E_F$ with respect to the CB edge, hence $\Phi_e$ reduces for $F > 0$ [becoming even negative (c)], while increases for $F < 0$ (a).

A similar analysis is performed also for the MoS₂-Au system, whose results are reported in Fig. 7. Also in this case, the external electric field effectively shifts $E_F$ inside the MoS₂ bandgap. However, the applied $F$ values depicted in Fig. 7 are not sufficient to zero the SBH for holes (a) and more negative electric fields are required to ease the contact to the VB of the MoS₂ [17].
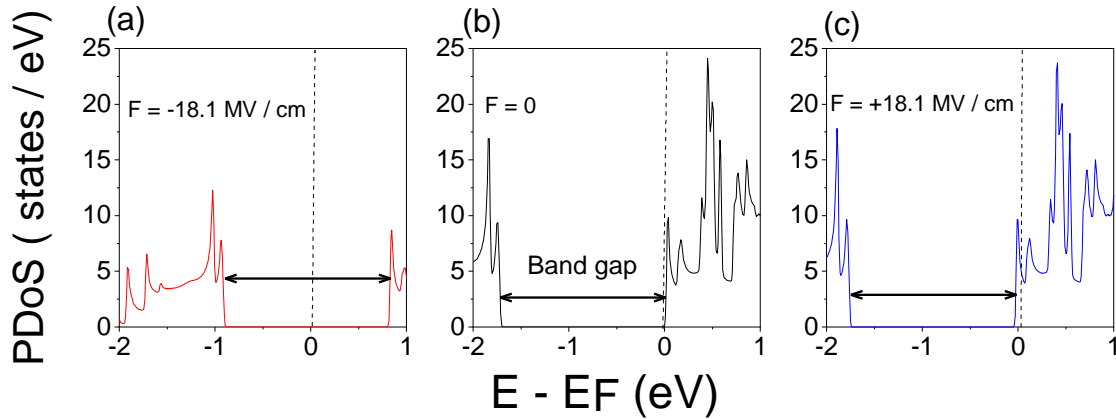


*Fig. 6: PDoS of MoS₂ in the back-gated MoS₂-Al contact featuring d = 0.8 nm when applying (a) F = −18.1 MV/cm, (b) F = 0, and (c) F = +18.1 MV/cm. Since the $E_F$ is de-pinned, the field effectively shifts $E_F$ with respect to the CB and VB edges of MoS₂ (n-type contact obtained for F > 0).*
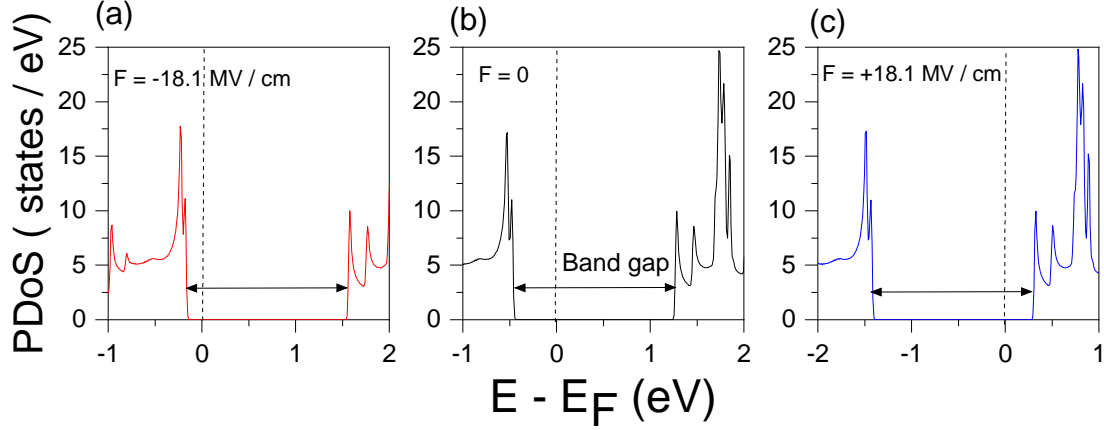
*Fig. 7: PDoS of MoS$_2$ in the back-gated MoS$_2$-Au contact featuring d = 0.8 nm when applying (a) F = −18.1 MV/cm, (b) F = 0, and, (c) F = +18.1 MV/cm. Since E$_F$ is de-pinned, the field shifts E$_F$ with respect to the CB and VB edges of MoS$_2$.*

In order to improve the understanding of the physical mechanism responsible for the observed E$_F$ shift, we extracted the charge induced by $F$ in the MoS$_2$ layer. For the charge evaluation we either used the Bader analysis [19, 27] or we simply employed the Gauss law. Indeed, for $d = 0.8$ nm, a dependable $F$ value can be determined at both sides of MoS$_2$ from the potential energy profile (see Fig. 7 of [17]). The charges extracted by means of the Bader analysis or the Gauss law agree well for both the MoS$_2$-Al [Fig. 8(a)] and MoS$_2$-Au systems (b). As expected, an electric field $F > 0$ increases the electron density in MoS$_2$ and eases the contact to the MoS$_2$ CB in the MoS$_2$-Al system. For a sufficiently large negative field, instead, in the MoS$_2$-Au contact it becomes possible to zero the SBH to the VB of the MoS$_2$. In this respect, it is worth mentioning that the apparently large $F$ values in Fig. 8 needed to induce $n$-type or $p$-type contacts are due to the use of vacuum as a spacer between the MoS$_2$ and the back-gate. Of course, by exploiting the dielectrics typically available in CMOS technologies, the required field can be reduced by a factor equal to the corresponding relative permittivity, namely about 4 for SiO$_2$ and about 30 for HfO$_2$, which is important in the view of limiting the tunneling current towards the back gate and preserving the reliability of the back gate dielectric.
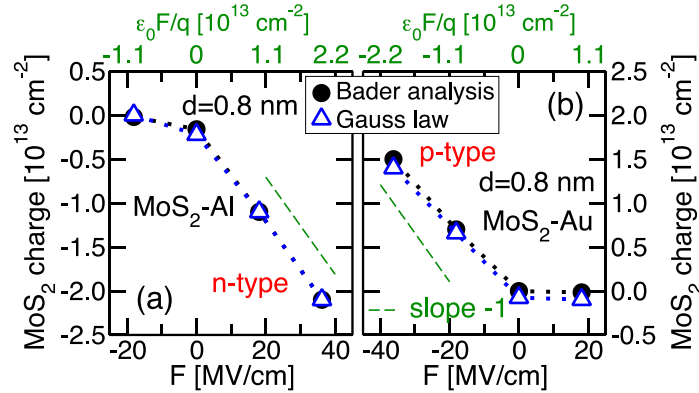


*Fig. 8: MoS$_2$ charge vs. F extracted with Bader analysis or through the Gauss law for the MoS$_2$-Al (a) and MoS$_2$-Au (b) systems. A large enough electric field applied through the back-gate induces either a n-type (a) or a p-type contact (b) in the two systems.*

## 5. MoS$_2$ contact with buffer layers

In the previous section, we have demonstrated how it is possible to effectively suppress the IGS induced by the metal proximity to MoS$_2$, thus resulting in the Fermi level de-pinning. In particular, by modulating the distance

between the MoS$_2$ and the metal, the SBH for electrons and holes can be engineered by choosing the proper metal WF and the possible use of a back gate to bias the system [24]. In this respect, the control of the distance between the contact and the semiconductor may be possible through the insertion of very thin buffer layers like, for instance, 2D materials. Such a possible engineering of the metal-MoS$_2$ contacts has been in fact explored in the recent literature, reporting that the use of 2D dielectrics or semimetals in between the metal and the MoS$_2$ reduces the measured contact resistance with respect to the case of the pure metal-MoS$_2$ system [26, 27, 29-31].

Therefore, we used the methodology described in Secs. 2 and 3 to study also MoS$_2$ contacts employing buffer layers. In particular, we examined different material systems to obtain either an *n*-type or a *p*-type Ohmic contact to the MoS$_2$.

### a) *n*-type contacts to MoS$_2$

Figure 4 shows that, under conditions for which the FLP is suppressed, it is possible to obtain a negligible SBH in the Al-MoS$_2$ contact, thus enabling an *n*-type Ohmic contact. In order to investigate a technologically viable option to de-pin the Fermi level in the MoS$_2$-Al heterostructure, we inserted an intermediate buffer monolayer between the metal and the 2D semiconductor, trying to ensure a sufficient MoS$_2$-Al spacing. Figure 9 shows the simulated supercell with the inserted h-BN dielectric. We matched the $\sqrt{3} \times \sqrt{3}$ MoS$_2$ supercell to a $2 \times 2$ supercell for the monolayer h-BN and then we added on top the 111 surface of the Al slab. Also in this case, the strain of the layers is small and, after relaxation of the structure, we obtained a separation between the Al slab and the MoS$_2$ of about $d = 0.71$ nm, a distance that should avoid the formation of IGS according to the analysis in Sec. 3.

A very similar procedure has been performed to analyze the contact with a graphene buffer. Again, we matched the $\sqrt{3} \times \sqrt{3}$ MoS$_2$ lattice to a $2 \times 2$ graphene monolayer crystal, obtaining a supercell that is equivalent to the one in Fig. 9. Relaxation of the structure led to a MoS$_2$-Al separation of $d = 0.695$ nm, thus ensuring a distance which may limit FLP.
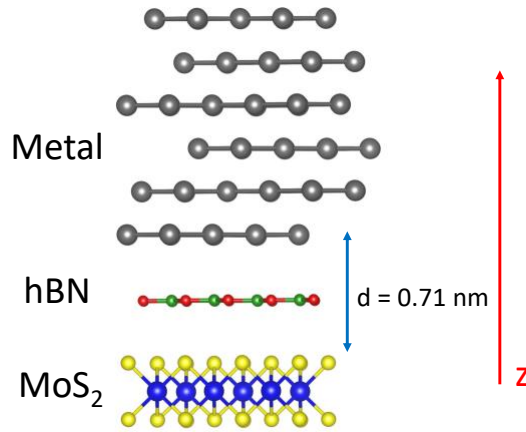


*Fig. 9: Simulated supercell of the contact featuring h-BN as buffer layer between MoS$_2$ and the metal slab.*

In Fig. 10 we have reported the MoS$_2$ PDoS for the bare MoS$_2$-Al system at MD or $d = 0.8$ nm and the results for the Al contacts featuring a h-BN dielectric or graphene as buffer layers. As it can be noted, the h-BN film (red line) can drastically suppress the densities of IGS compared to the minimum distance MoS$_2$-Al system, thus allowing the $E_F$ de-pinning, and the corresponding negligible SBH is in agreement with the Schottky–Mott rule and it is essentially the same as in the system having a vacuum distance $d = 0.8$ nm. Such a drastic reduction of the SBH is a promising path towards an Ohmic *n*-type contact to MoS$_2$, but it should be noted that the presence of the h-BN buffer layer may deteriorate the electron transmission coefficient across the heterostructure with respect to the MoS$_2$-Al system at MD. However, the experimental data reported in the literature suggest that such a possible degradation of the electronic transmission is overcompensated by the SBH suppression enabled by the Fermi level de-pinning, thus resulting in an overall improvement of the contact resistance [31].
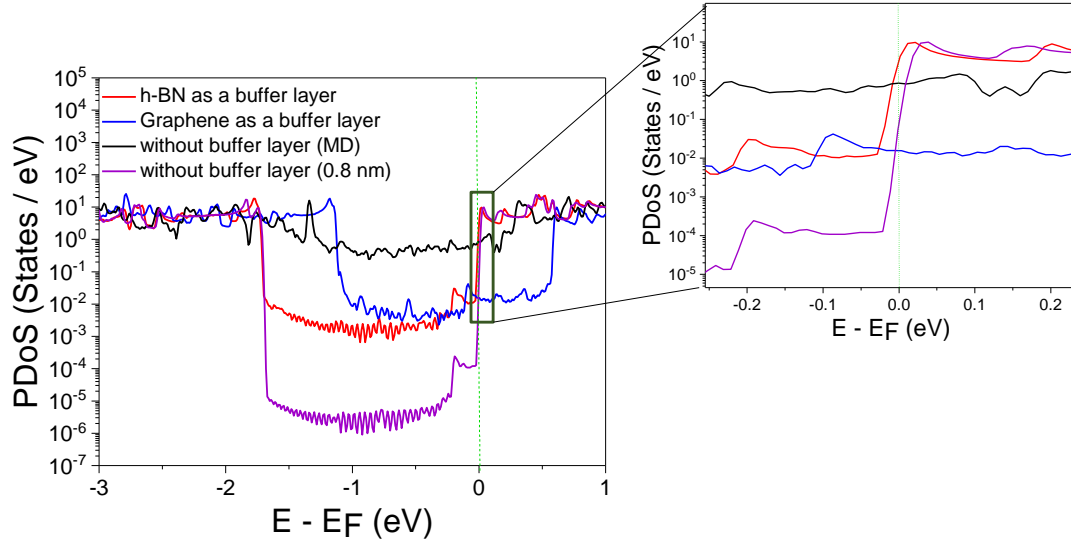
*Fig. 10: PDoS of the MoS₂ in MoS₂-Al contacts with or without buffer layers. Graphene or h-BN dielectric have been selected as buffer layers.*

The MoS$_2$ PDoS for the contact featuring the graphene as buffer layer, illustrated by the blue line in Fig. 10, shows that, in this case, the Fermi level is located well inside the MoS$_2$ bandgap and the SBH is large to both the conduction and valence bands. This behavior does not seem to be due to the IGS, whose density is only slightly larger with respect to the h-BN case, but it is more probably due to the metal-graphene interaction. Indeed, the semi-metallic nature of graphene may result in a significant charging of the graphene layer, which is instead expected to be negligible for the insulating h-BN film. So, apparently the use of graphene as buffer layer is less effective to reduce the electron SBH with respect to the h-BN case when Al is used as metal contact.

To gain more insight into the different behavior of the graphene and the h-BN as buffer layers, we employed the Bader analysis to evaluate the metal induced doping of MoS$_2$ in the two contact options. For the h-BN buffer layer, the Al contact charges the MoS$_2$ with a large electron density of about $n = 1.7 \cdot 10^{13}$ cm$^{-2}$, which reflects the position of $E_F$ in proximity of the CB edge (Fig. 10, red line).

The Bader analysis for the contact with the graphene buffer layer revealed that, instead, the Al slab can induce a large electron charge in graphene ($n \sim 7 \cdot 10^{13}$ cm$^{-2}$), while the corresponding charge in MoS$_2$ is only about $n = 3.5 \cdot 10^{12}$ cm$^{-2}$, in qualitative agreement with the $E_F$ being well below the CB edge. So, in this case, the graphene tends to screen the MoS$_2$, preventing its charging, most probably because of the graphene semi-metal nature. However, experiments in the literature have shown a reduced contact resistance when inserting graphene between the metal contact and MoS$_2$ [26]. This may be due to the reduction of IGS with respect to the metal-MoS$_2$ system at the minimum distance (Fig. 10, black line) and/or to a better electron transmission across the heterostructure, taking advantage of the semi-metal nature of graphene.

### b) *p*-type contacts to MoS$_2$

A h-BN buffer layer may be instrumental to suppress FLP and attain an Ohmic behavior even in *p*-type contacts to MoS$_2$, as it is illustrated also in Figs. 2 and 3. However the electron affinity and energy bandgap of MoS$_2$ makes it very challenging to push the Fermi level down to the VB of MoS$_2$ even for high WF metals, such as Au and Pd [24]. Also the analysis in Figs. 2 and 3 of this paper shows that the SBH for holes remains large, except for the case of a very large and negative electric field induced through a back-gate contact (see Fig. 8) [17].

In Ref. [24, 32] the authors have proposed the use of metallic 2D monolayers with high WF to achieve a good contact to the VB of the 2D semiconductors. Stimulated by these reports, we here explored the characteristics of MoS$_2$-Au contacts featuring an intermediate NbS$_2$ buffer monolayer (WF = 6.1 eV) [24]. Since NbS$_2$ has the same crystal structure as MoS$_2$ and a very similar lattice constant [32], the simulated supercell matches the $\sqrt{3} \times \sqrt{3}$

MoS$_2$ cell with an equivalent $\sqrt{3} \times \sqrt{3}$ NbS$_2$ monolayer. Again, the 2D crystal of MoS$_2$ and NbS$_2$ is matched with the 111 surface of the Au slab.

Figure 11 reports the PDoS on MoS$_2$ and on NbS$_2$ for the MoS$_2$-NbS$_2$-Au contact. The $E_F$ position inside the bandgap of MoS$_2$ is consistent with the results in Fig. 2(a), indicating the de-pinning of the Fermi level and leading to a similar SBH for holes of about 0.47 eV. However, states inside the MoS$_2$ bandgap clearly appear in the MoS$_2$ - NbS$_2$ - Au system (Fig. 11, blue curve). The authors in [24, 32] argued that such states belong to MoS$_2$ and that, because of their continuity towards the MoS$_2$ VB, they may bridge the MoS$_2$ to the NbS$_2$ VB (pink curve), thus realizing an Ohmic *p*-type contact. From the analysis of the PDoS reported in the present study it is not possible to confirm or dispute any hypothesis about the electronic transport through the heterostructure, which demands for a more advanced analysis including also transport simulations. This goes beyond the scope of the present paper, which leaves an uncertainty about the actual SBH value for the holes in the contact featuring Au and NbS$_2$.
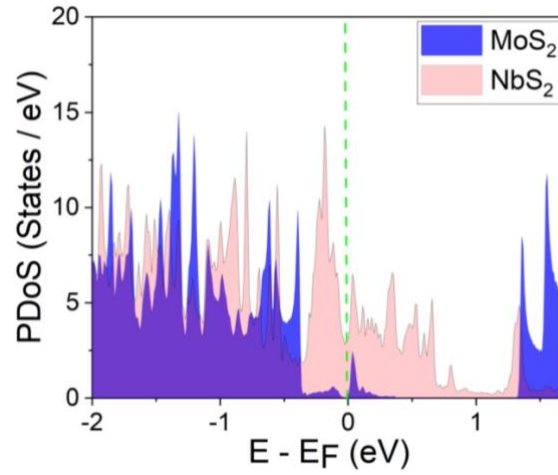


*Fig. 11: PDoS of the MoS$_2$ and of the NbS$_2$ in the MoS$_2$-NbS$_2$-Au contact.*

### 6. Conclusions

We have reported a detailed DFT analysis of FLP and SBH for defect-free contacts to MoS$_2$ featuring different metals and buffer layers. The study provided useful insights for the attainment of an Ohmic metal-MoS$_2$ contact.

For a defect-free MoS$_2$ layer, the metal-MoS$_2$ distance *d* is the crucial parameter that should be controlled in order to prevent the FLP. By ensuring a sufficient distance, the IGS formation and the resulting FLP can be effectively suppressed, thus enabling the modulation of the SBH through the choice of the metal WF, as well as a further SBH adjustment via the back-gating of the contact structure.

The insertion of a buffer layer between the metal and the MoS$_2$ is a technologically viable means to control the metal-MoS$_2$ distance. We explored solutions using graphene or h-BN spacer layers for the Al contact and our simulation have shown that h-BN can effectively suppress the FLP and result in a presumably zero-SBH Ohmic *n*-type contact. The system with graphene, instead, reveals a that FLP is still present, thus reducing the advantage of the semi-metal characteristics of graphene. This is essentially due to the screening of the MoS$_2$ exerted by graphene, that prevents the charging of MoS$_2$.

For the MoS$_2$-Au contact we also explored a previously proposed pathway to the *p*-type contact consisting in the insertion of the metallic 2D NbS$_2$ monolayer as a buffer layer between Au and MoS$_2$. Also in this case, we see that the buffer layer can partly suppress the FLP; however, due to the onset of states close to the VB of MoS$_2$, we feel that an uncertainty persists about the value of SBH for this contact option. A more thorough analysis including the electronic transport across the heterostructure appears necessary to confirm the conjecture reported in [24, 32], according to which the states inside the MoS$_2$ bandgap could reduce the SBH for holes and ease the implementation of a *p*-type contact to the MoS$_2$.

## References

[1] Radisavljevic B, Radenovic A, Brivio J, Giacometti V, Kis A. Single-layer $MoS_2$ transistors. Nature nanotechnology. 2011 Mar;6(3):147-50.

[2] Hosseini M, Elahi M, Pourfath M, Esseni D. Strain-Induced Modulation of Electron Mobility in Single-Layer Transition Metal Dichalcogenides $MX_2$ ($M$ = Mo, W; $X$ = S, Se). IEEE Trans. on Electron Devices. 2015 Aug 10;62(10):3192-8.

[3] Rus D, Tolley MT. Design, fabrication and control of soft robots. Nature. 2015 May;521(7553):467-75.

[4] Chortos A, Liu J, Bao Z. Pursuing prosthetic electronic skin. Nature materials. 2016 Sep;15(9):937-50.

[5] Khan A.I., Khakbaz P, Brenner K.A., Smithe K.K., Mleczko M.J., Esseni D., Pop E. Large temperature coefficient of resistance in atomically thin two-dimensional semiconductors. Applied Physics Letters. 2020 May 18;116(20):203105.

[6] Iannaccone G, Bonaccorso F, Colombo L, Fiori G. Quantum engineering of transistors based on 2D materials heterostructures. Nature nanotechnology. 2018 Mar;13(3):183-91.

[7] International Roadmap for Devices and Systems (IRDS), [Available online, accessed November 2021] : http://irds.ieee.org/.

[8] Fang Q, Zhao X, Yuan L, Wang B, Xia C, Ma F. Non-invasively improving the Schottky barrier of $MoS_2$/metal contacts by inserting a SiC layer. Physical Chemistry Chemical Physics. 2021;23(27):14796-802.

[9] English CD, Shine G, Dorgan VE, Saraswat KC, Pop E. Improved contacts to $MoS_2$ transistors by ultra-high vacuum metal deposition. Nano letters. 2016 Jun 8;16(6):3824-30.

[10] Tung RT. The physics and chemistry of the Schottky barrier height. Applied Physics Reviews. 2014 Mar 13;1(1):011304.

[11] Kim C, Moon I, Lee D, Choi MS, Ahmed F, Nam S, Cho Y, Shin HJ, Park S, Yoo WJ. Fermi level pinning at electrical metal contacts of monolayer molybdenum dichalcogenides. ACS nano. 2017 Feb 28;11(2):1588-9.

[12] Allain A, Kang J, Banerjee K, Kis A. Electrical contacts to two-dimensional semiconductors. Nature materials. 2015 Dec;14(12):1195-205.

[13] Wang Y, Chhowalla M. Making clean electrical contacts on 2D transition metal dichalcogenides. Nature Reviews Physics. 2021 Dec 3:1-2.

[14] Kang J, Liu W, Sarkar D, Jena D, Banerjee K. Computational study of metal contacts to monolayer transition-metal dichalcogenide semiconductors. Physical Review X. 2014 Jul 14;4(3):031005.

[15] Farmanbar M, Brocks G. First-principles study of van der Waals interactions and lattice mismatch at $MoS_2$/metal interfaces. Physical Review B. 2016 Feb 2;93(8):085304.

[16] Guo Y, Liu D, Robertson J. 3D behavior of Schottky barriers of 2D transition-metal dichalcogenides. ACS applied materials & interfaces. 2015 Nov 25;7(46):25709-15.

[17] Khakbaz P, Driussi F, Giannozzi P, Gambi A, Esseni D. Simulation study of Fermi level depinning in metal-$MoS_2$ contacts. Solid-State Electronics. 2021 May 27:108039.

[18] Giannozzi P, et al. Advanced capabilities for materials modelling with Quantum ESPRESSO. Journal of Physics: Condensed Matter. 2017 Oct 24;29(46):465901.

[19] Driussi F, Venica S, Gahoi A, Gambi A, Giannozzi P, Kataria S, Lemme MC, Palestri P, Esseni D. Improved understanding of metal–graphene contacts. Microelectronic Engineering. 2019 Aug 15; 216:111035.

[20] Khakbaz P, Driussi F, Gambi A, Giannozzi P, Venica S, Esseni D, Gaho A, Kataria S, Lemme M. C. DFT study of graphene doping due to metal contacts. Proceedings of SISPAD. September 2019. 1-4.

[21] Brumme T, Calandra M, Mauri F. Electrochemical doping of few-layer ZrNCl from first principles: Electronic and structural properties in field-effect configuration. Physical Review B. 2014 Jun 6;89(24):245406.

[22] Zhong H, Quhe R, Wang Y, Ni Z, Ye M, Song Z, Pan Y, Yang J, Yang L, Lei M, Shi J. Interfacial properties of monolayer and bilayer $MoS_2$ contacts with metals: beyond the energy band calculations. Scientific reports. 2016 Mar 1 ;6(1) :1-6.

[23] Li T, Galli G. Electronic properties of $MoS_2$ nanoparticles. The Journal of Physical Chemistry C. 2007 Nov 8;111(44):16192-6.

[24] Farmanbar M, Brocks G. Ohmic contacts to 2D semiconductors through van der Waals bonding. Advanced electronic materials. 2016 Apr;2(4):1500405.

[25] Bruix A, Miwa JA, Hauptmann N, Wegner D, Ulstrup S, Grønborg SS, Sanders CE, Dendzik M, Čabo AG, Bianchi M, Lauritsen JV. Single-layer MoS 2 on Au (111): Band gap renormalization and substrate interaction. Physical Review B. 2016 Apr 18;93(16):165422.

[26] Qiu D, Kim E K. Electrically tunable and negative Schottky barriers in multi-layered graphene/$MoS_2$ heterostructured transistors. Scientific reports. 2015 Sep 3;5(1):1-7.

[27] Park, W., Min, J.-W., Shaikh, S.F. and Hussain, M.M. (2017), Stable $MoS_2$ Field-Effect Transistors Using $TiO_2$ Interfacial Layer at Metal/MoS2 Contact. Phys. Status Solidi A, 214: 1700534. https://doi.org/10.1002/pssa.201700534.

[28] Henkelman G, Arnaldsson A, Jónsson H. A fast and robust algorithm for Bader decomposition of charge density. Computational Materials Science. 2006 Jun 1;36(3):354-60.

[29] Kaushik N, Karmakar D, Nipane A, Karande S, Lodha S. Interfacial n-doping using an ultrathin $TiO_2$ layer for contact resistance reduction in $MoS_2$. ACS applied materials & interfaces. 2016 Jan 13;8(1):256-63.

[30] Wang, J., Yao, Q., Huang, C.-W., Zou, X., Liao, L., Chen, S., Fan, Z., Zhang, K., Wu, W., Xiao, X., Jiang, C. and Wu, W.-W. (2016), High Mobility $MoS_2$ Transistor with Low Schottky Barrier Contact by Using Atomic Thick h-BN as a Tunneling Layer. Adv. Mater., 28: 8302-8308. DOI: 10.1002/adma.201602757.

[31] Kim GS, Kim SH, Park J, Han KH, Kim J, Yu HY. Schottky barrier height engineering for electrical contacts of multilayered MoS2 transistors with reduction of metal-induced gap states. ACS nano. 2018 May 31;12(6):6292-300.

[32] Ding X, Zhang S, Zhao M, Xiang Y, Zhang KH, Zu X, Li S, Qiao L. NbS 2: A promising p-type ohmic contact for two-dimensional materials. Physical Review Applied. 2019 Dec 30;12(6):064061.